lo ma

Marc O. Delchini[a], Jean C. Ragusa[*,a], Ray A. Berry[b]

[a]*Department of Nuclear Engineering, Texas A&M University, College Station, TX 77843, USA*
[b]*Idaho National Laboratory, Idaho Falls, ID 83415, USA*

Abstract

aaa

Key words: aaa, bbb, ccc

1. Introduction

Over the past years an increasing interest raised for computational methods that can solve both compressible and incompressible flows. In engineering applications, there is often the need to solve for complex flows where a near incompressible regime or low Mach flow coexists with a supersonic flow domain. For example, such flow are encountered in aerodynamic in the study of airships. In the nuclear industry, flows are nearly the incompressible regime but compressible effects cannot be neglected because of the heat source and thus needs to be accurately resolved.
Because of the hyperbolic nature of the flow equations, numerical methods are required in order to accurately resolve shocks that can form during transonic and supersonic flows. Numerous numerical methods are available in the literature: flux-limiter, pressure-based viscosity method, Lapidus method, the entropy-viscosity method among others. These numerical methods are usually tested and developed using simple equation of states and for transonic and supersonic flows where the disparity between the acoustic waves and the fluid speed is not large since the Mach number is of order one.

2. The Entropy Viscosity Method

2.1. Background

In this section, the entropy-based viscosity method [3, 4, 5] is recalled for the multi-D Euler equations (with constant area A) [1]. As mentioned in Section 1 the entropy-based viscosity method consists of adding dissipative terms, with

---

[*]Corresponding author
Email addresses: `delchmo@tamu.edu` (Marc O. Delchini), `jean.ragusa@tamu.edu` (Jean C. Ragusa), `ray.berry@inl.gov` (Ray A. Berry)

a viscosity coefficient modulated by the entropy production which allows high-order accuracy when the solution is smooth. Thus, two questions arise: (i) how are the viscosity dissipative terms derived and (ii) how to numerically compute the entropy production. Answers to the first question can be found in [2] by Guermond et al., that details the proof leading to the derivation of the artificial dissipative terms (Eq. (1)) consistent with the entropy minimum principle theorem. The viscous regularization obtained is valid for any equation of state as long as the opposite of the physical entropy function is convex.

$$
\begin{cases}
\partial_t \left(\rho \right) + \vec{\nabla} \cdot (\rho \vec{u}) = \vec{\nabla} \cdot \left(\kappa \vec{\nabla} \rho \right) \\
\partial_t \left(\rho \vec{u} \right) + \vec{\nabla} \cdot (\rho \vec{u} \otimes \vec{u} + P\mathbf{I}) = \vec{\nabla} \cdot \left(\mu \rho \vec{\nabla}^s \vec{u} + \kappa \vec{u} \otimes \vec{\nabla} \rho \right) \\
\partial_t \left(\rho E \right) + \vec{\nabla} \cdot [\vec{u} \left(\rho E + P \right)] = \vec{\nabla} \cdot \left(\kappa \vec{\nabla} \left(\rho e \right) + \frac{1}{2} ||\vec{u}||^2 \kappa \vec{\nabla} \rho + \rho \mu \vec{u} \vec{\nabla} \vec{u} \right) \\
P = P \left(\rho, e \right)
\end{cases}
\tag{1}
$$

where κ and μ are local positive viscosity coefficients.

The existence of a specific entropy s, function of the density ρ and the internal energy e is assumed. Convexity of $-s$ with respect to e and $1/\rho$ is required, along with the following equality verified by the partial derivatives of s: $P\partial_e s + \rho^2 \partial_\rho s = 0$.

One crucial step remains a definition for the local viscosity coefficients μ and κ. In the current version of the method, κ and μ are set equal, so that the above viscous regularization (Eq. (1)) is equivalent to the parabolic regularization [8]. The current definition includes a first-order viscosity coefficient referred to with the subscript max, and a high-order viscosity coefficient referred to with the subscript e. The first-order viscosity coefficients μ_{max} and κ_{max} are proportional to the local largest eigenvalue $||\vec{u}|| + c$ and equivalent to an upwind-scheme, when used, which is known to be over-dissipative and monotone [7]:

$$
\mu_{max}(\vec{r}, t) = \kappa_{max}(\vec{r}, t) = \frac{h}{2} \left(||\vec{u}|| + c \right),
\tag{2}
$$

where h is the spatial grid size.

The second-order viscosity coefficients κ_e and μ_e are set proportional to the entropy production that is evaluated by computing the local entropy residual D_e. It also includes the interfacial jump of the entropy flux J that will allow to detect any discontinuities other than shocks:

$$
\mu_e(\vec{r}, t) = \kappa_e(\vec{r}, t) = h^2 \frac{\max \left(|D_e(\vec{r}, t)|, J \right)}{||s - \bar{s}||_\infty} \text{ with } D_e(\vec{r}, t) = \partial_t s + \vec{u} \cdot \vec{\nabla} s
\tag{3}
$$

where $|| \cdot ||_\infty$ and $\bar{\cdot}$ denote the infinite norm operator and the average operator over the entire computational domain, respectively. The definition of the jump J is discretization-dependent and examples of definition can be found in [1] for DGFEM. The denominator $||s - \bar{s}||_\infty$ is used for dimensionality purposes and should not be of the same order as h, on penalty of loosing the high-order accuracy. Currently, there are no theoretical justification for choosing the

denominator.

The definition of the viscosity coefficients μ and κ is function of the first- and second-order viscosity coefficients as follows:

$$\mu(\vec{r}, t) = \min\left(\mu_e(\vec{r}, t), \mu_{max}(\vec{r}, t)\right) \text{ and } \kappa(\vec{r}, t) = \min\left(\kappa_e(\vec{r}, t), \kappa_{max}(\vec{r}, t)\right). \quad (4)$$

This definition allows the following properties. In shock regions, the second-order viscosity coefficient experiences a peak because of entropy production, and thus, saturates to the first-order viscosity that is known to be over-dissipative and will smooth out oscillations. Anywhere else, the entropy production being small, the viscosity coefficients μ and κ are of order h^2.

Using the above definition of the entropy-based viscosity method, high-order accuracy was demonstrated and excellent results were obtained with 1-D Sod shock tubes and various 2-D tests [3, 4, 1].

2.2. Issues in the Low-Mach Regime

In the Low-Mach Regime, the flow is known to be isentropic resulting in very little entropy production. Since the entropy viscosity method is directly based on the evaluation of the local entropy production, it will be interested to study how the entropy viscosity coefficients μ and κ scale in the low Mach regime. Mathematically, it means that the entropy residual D_e will be very small, so will be the denominator $||s - \bar{s}||_\infty$, thus making the ratio, used in the definition of the viscosity coefficients Eq. (3), undetermined. Therefore, the current definition of the viscosity coefficients seems unadapted to subsonic flow and could lead to ill-scaled dissipative terms. A solution would be to recast the entropy residual as a function of other variables in order to have more freedom in the choice of the normalization parameter. The idea is to still define the viscosity coefficient proportional to the entropy residual that is a good indicator of the flow type (subsonic or supersonic).

2.3. The dissipative-terms for the multi-D Euler equations with variable area

One of the focus of this paper is to investigate the application of the entropy viscosity method to the multi-D Euler equations with variable area: first, the dissipative terms are derived following (REF), and, the viscosity coefficients are defined. The full derivation can be found in APPENDIX and only the main steps are given here. The objective here is to assess wether or not the entropy viscosity method will accurately resolve a flow in a 1-D convergent-divergent nozzle (REFS with mine). In Section 5, 1-D results for liquid water in a nozzle are shown. This test is interested for two reasons: (i) the flow under consideration is subsonic which is the focus of this paper, and, (ii) the flow reaches a steady-state and an exact-solution can be derived for this particular case (REF). Thus, a convergence study will be performed in order to show second-order accuracy.

The multi-D Euler equations degenerate to the multi-D Euler equations given in Eq. (1) when assuming constant area. The main difference lies in the momentum equation that contains a non-conservative terms in the right-hand side. For the

purpose of this paper, the variable area is denoted by $A(\vec{r})$ and is only spatial dependent. The multi-D Euler equations with variable area are recalled (REF):

$$\begin{cases} \partial_t\left(\rho A\right) + \vec{\nabla}\cdot(\rho\vec{u}A) = 0 \\ \partial_t\left(\rho\vec{u}A\right) + \vec{\nabla}\cdot[A\left(\rho\vec{u}\otimes\vec{u}+P\mathbf{I}\right)] = P\vec{\nabla}A \\ \partial_t\left(\rho E\right) + \vec{\nabla}\cdot[\vec{u}\left(\rho E+P\right)] = 0 \end{cases} \tag{5}$$

This system (Eq. (5)) admits the following entropy equation with the same entropy function as defined previously in Section 2.1:

$$\rho A\left(\partial_t s + \vec{u}\cdot\vec{\nabla}s\right) = 0$$

Once again, by adding dissipative terms in each equation of Eq. (5), the entropy equation is modified and by invoking the entropy minimum principle, adequate definition of the dissipative terms are derived as shown in Eq. (6):

$$\begin{cases} \partial_t\left(\rho A\right) + \vec{\nabla}\cdot(\rho\vec{u}A) = \vec{\nabla}\cdot\left(A\kappa\vec{\nabla}\rho\right) \\ \partial_t\left(\rho\vec{u}A\right) + \vec{\nabla}\cdot[A\left(\rho\vec{u}\otimes\vec{u}+P\mathbf{I}\right)] = P\vec{\nabla}A + \vec{\nabla}\cdot\left[A\left(\mu\rho\vec{\nabla}^s\vec{u}+\kappa\vec{u}\otimes\vec{\nabla}\rho\right)\right] \\ \partial_t\left(\rho E\right) + \vec{\nabla}\cdot[\vec{u}\left(\rho E+P\right)] = \vec{\nabla}\cdot\left[A\left(\kappa\vec{\nabla}\left(\rho e\right)+\frac{1}{2}||\vec{u}||^2\kappa\vec{\nabla}\rho+\rho\mu\vec{u}\vec{\nabla}\vec{u}\right)\right] \end{cases} \tag{6}$$

The dissipative terms are very similar to the ones obtained for the multi-D Euler equations: each dissipative flux is multiplied by the variable area A in order to ensure conservation of the flux. When assuming a constant area, Eq. (1) is retrieved.

The definition of the viscosity coefficients is explained in Section 3.2. It is expected to have the same definition of the viscosity coefficients between the multi-D Euler equations with variable and constant area. This assumption is justified by the entropy residual for the variable area case: it can be obtained by simply multiplying the entropy residual of Eq. (3) by the area A. Thus, the variations of the entropy residual should be identical.

3. All-speed Reformulation of the Entropy Viscosity Method

In this section, it is shown how the entropy residual D_e can be recast as a function of the pressure, the density and the speed of sound. Then, an low Mach asymptotic study of the multi-D Euler equations is performed in order to derive the correct normalization parameter.

3.1. New Entropy Production Residual

The first step in defining a viscosity coefficient that behaves well in the low mach limit is to recast the entropy residual in terms of thermodynamic variables:

$$D_e(\vec{r},t) = \partial_t s + \vec{u}\cdot\vec{\nabla}s = \frac{s_e}{P_e}\left(\underbrace{\frac{dP}{dt}-c^2\frac{d\rho}{dt}}_{\tilde{D}_e(\vec{r},t)}\right), \tag{7}$$

4

where $\frac{d\cdot}{dt}$ denotes the material or total derivative, and P_e is the partial derivative of pressure with respect to internal energy. The steps that lead to the new formulation of the entropy residual D_e can be found in APPENDIX.

The entropy residual D_e and $\tilde{D}_e$ are proportional to each other and therefore will experience the same variation when taking the absolute value. Thus, locally evaluating $\tilde{D}_e$ instead of D_e should allow us to measure the entropy production point wise. This new expression given in Eq. (7) has multiple advantages:

- an analytical expression of the entropy function is not longer needed: the entropy residual $\tilde{D}_e$ is evaluated using the local values of the pressure, the density and the speed of sound. Deriving an entropy function for some complex equation of states can be difficult.

- with the proposed expression of the entropy residual function of pressure and density, additional normalizations suitable for low Mach flows of the entropy residual can be devised. Examples include the pressure itself, or combination of the density, the speed of sound and the norm of the velocity: ρc^2, $\rho c ||\vec{u}||$ and $\rho ||\vec{u}||^2$.

The viscosity coefficients μ and κ are now defined proportional to the new entropy residual $\tilde{D}_e$ on the model of Eq. (3) as follows:

$$\mu\left(\vec{(r)},t\right) = \kappa\left(\vec{(r)},t\right) = h^2 \frac{\max\left(\tilde{D}_e, J\right)}{n(P)} \qquad (8)$$

where $n(P)$ is a normalization parameter to determine and all other variables were defined previously.

As mentioned earlier, the normalization parameter $n(P)$ must be of the same units as the pressure for the viscosity coefficients to have the unit of a dynamic viscosity (m^2/s). Multiples options are available to us (P, ρc^2, $\rho c ||\vec{u}||$ and $\rho ||\vec{u}||^2$). The choice of the normalization parameter cannot be random if the definition of the viscosity coefficient is wanted to be well-scaled for a wide range of Mach numbers. For example, by choosing $n(P) = \rho ||\vec{u}||^2$, the viscosity coefficient will become very large as the Mach number decreases which would be unnecessary since the equations will not develop any shock or discontinuity. Therefore, it is proposed to carry, in Section 3.2, a low-Mach asymptotic study of the multi-D Euler equations in order to determine the correct expression for the normalization parameter $n(P)$.

3.2. Low-Mach asymptotic study of the multi-D Euler equations

The asymptotic study requires the multi-D Euler equations to be non dimensionalized: the objective is to make the Mach number appears and thus, use a polynomial expansion of the variables as a function of the Mach number in order to derive the leading, first- and second-order equations. Before detailing the steps of the asymptotic method, let us have a closer look at the system of equations under consideration. The initial system of equations is composed of the multi-D Euler equations. For stability purpose, artificial dissipative terms

are added to each equation as explained in Section 2. The resulting system of equations is alike the multi-D Navier-Stokes equations in a sense that it contains second-order derivative terms. Thus, it would be interesting to look at the steps employed in the asymptotic study of the multi-D Navier-Stokes equations in order to understand how the dissipative terms are treated. Fortunately, this process is well-documented in the literature (REFS) for both multi-D Euler equations and Navier-Stokes equations. The work presented here is mainly inspired of (REF) that focuses on the asymptotic study in the low Mach regime of Navier-Stokes equations. During the derivation, the reader has to keep in mind that the objective of this section is to derive a normalization parameter for the definition of the viscosity coefficients so that the multi-D Euler equations degenerate to the incompressible system of equations, which implies that the dissipative terms are well-scaled. The full derivation that leads to the final result can be found in APPENDIX. In this section, only the main steps are recalled.

To express Eq. (1) in dimensionless variables, the following definitions are used

$$
\begin{aligned}
\rho &= \frac{\rho^*}{\rho_\infty},\ P = \frac{P^*}{\rho_\infty c_\infty^2},\ \mu = \frac{\mu^*}{\mu_\infty},\ ,\ E = \frac{E^*}{c_\infty^2},\ \mu = \frac{\mu^*}{\mu_\infty}, \\
\kappa &= \frac{\kappa^*}{\kappa_\infty},\ x = \frac{x^*}{L_\infty},\ t = \frac{t^*}{L_\infty/u_\infty},\ u = \frac{u^*}{u_\infty}
\end{aligned}
\tag{9}
$$

where the subscript ∞ and the upper script $*$ denote far field or stagnation quantities and the dimensionless variables, respectively. The reference quantities are chosen such that the non dimensional flow quantities are of order one for any low reference-Mach number

$$
M_\infty = \frac{u_\infty^*}{c*_\infty}
\tag{10}
$$

where c_∞^* is a reference value for the speed of sound.

Then, using the non dimensional quantities and the multi-D Euler equations from Eq. (1) , the following non dimensional form is obtained:

$$
\begin{cases}
\partial_t \rho + \nabla \left(\rho \vec{u} \right) = \frac{1}{Re_\infty Pr_\infty} \nabla \cdot \left(\kappa \nabla \rho \right) \\
\partial_t \left(\rho \vec{u} \right) + \nabla \left(\rho \vec{u} \otimes \vec{u} \right) + \frac{1}{M_\infty^2} \nabla \left(P \right) = \frac{1}{Re_\infty} \nabla \left(\rho \mu \nabla \vec{u} \right) + \frac{1}{Re_\infty Pr_\infty} \nabla \cdot \left(\vec{u} \otimes \kappa \nabla \rho \right) \\
\partial_t \left(\rho E \right) + \nabla \cdot \left[\vec{u} \left(\rho E + P \right) \right] = \frac{1}{Re_\infty Pr_\infty} \nabla \cdot \left(\kappa \nabla (\rho e) \right) + \frac{M_\infty^2}{Re_\infty} \nabla \cdot \left(\vec{u} \rho \mu \nabla \vec{u} \right) \\
+ \frac{M_\infty^2}{2 Re_\infty Pr_\infty} \nabla \cdot \left(\kappa u^2 \nabla \rho \right) \\
P = \left(\gamma - 1 \right) \left(\rho E + M_\infty^2 \rho u^2 \right)
\end{cases}
$$

where the *numerical* Reynolds (Re_∞) and Prandtl (Pr_∞) numbers are defined as follows:

$$
Re_\infty = \frac{u_\infty L_\infty}{\mu_\infty} \text{ and } Pr_\infty = \frac{\mu_\infty}{\kappa_\infty}.
\tag{11}
$$

Since it is chosen to have the same definition for both μ and κ the numerical Prandtl number is unconditionally equal to one: $Pr_\infty = 1$.

Once the dimensionless equations are obtained, the next step consists of expanding each variable in term of the Mach number (example given in Eq. (12) for the pressure P) in order to derive the leading, first- and second-order equations.

$$P(\vec{r},t) = P_0(\vec{r},t) + P_1(\vec{r},t)M_\infty + P_2(\vec{r},t)M_\infty^2 + \ldots \text{ with } M_\infty \to 0 \qquad (12)$$

Before deriving the leading-order equation, a choice needs to be made on how the numerical Reynolds number scales. Multiple options are available to us and a few example are given: $Re_\infty = M_\infty$, or $Re_\infty = M_\infty^{-1}$ or $Re_\infty = 1$. Let us assume for academy purpose that the numerical Reynolds number scales as the inverse of the Mach number square: $Re_\infty = M_\infty^{-2}$. The best way to evaluate the impact of this choice on the equations, is to look at the momentum equation and try to derive the order M_∞^{-2}:

$$\vec{\nabla} P_0 = \vec{\nabla} \cdot (\rho_0 \mu_0 \vec{\nabla} \vec{u}_0 + \vec{u}_0 \otimes \vec{\nabla} \rho_0) \qquad (13)$$

which is known to be (REF)

$$\vec{\nabla} P_0 = 0 \qquad (14)$$

It is clear that Eq. (13) and Eq. (14) will not yield the same result. The same conclusion is drawn when deriving the order M_∞^{-1} of the momentum equation, making our initial assumption not suitable. From the above result, it is understood that the numerical Reynolds number has to scale as one so that it does not affect the orders M_∞^{-2} and M_∞^{-1} of the momentum equations: $Re_\infty = 1$. Thus, with such assumption, Eq. (11) implies:

$$\text{At order } M_\infty^{-2}:$$
$$\vec{\nabla} P_0 = 0$$
$$\text{At order } M_\infty^{-1}:$$
$$\vec{\nabla} P_1 = 0$$
$$\text{At leading-order:}$$
$$\partial_t \rho_0 + \vec{\nabla} \cdot (\rho_0 \vec{u}_0) = \vec{\nabla} \cdot (\kappa_0 \vec{\nabla} \rho_0)$$
$$\partial_t (\rho_0 \vec{u}_0) + \vec{\nabla} \cdot (\rho_0 \vec{u}_0 \otimes \vec{u}_0) + \vec{\nabla} P_2 = \vec{\nabla} \cdot (\rho_0 \mu_0 \vec{\nabla} \vec{u}_0 + \vec{u}_0 \otimes \vec{\nabla} \rho_0)$$
$$\partial_t (\rho_0 E_0) + \vec{\nabla} \cdot [\vec{u}_0 (\rho_0 E_0 + P_0)] = \vec{\nabla} \cdot (\kappa_0 \vec{\nabla} (\rho_0 e_0))$$

Under this form, the dissipative terms are well-scaled and should not alter the physical solution in the asymptotic limit.

It is now determined that the numerical Reynolds number Re_∞ has to scale as one. Following Eq. (11), Re_∞ is a function of the μ_∞, and thus n_P. It can be shown using Eq. (9) and the definitions of $\tilde{D}$ given in Eq. (7) that:

$$\mu_\infty = \frac{\rho_\infty c_\infty^2 u_\infty L}{n_{P,\infty}} \qquad (15)$$

where $n_{P,\infty}$ is the far-field quantity for the normalization parameter n_P. Substituing Eq. (15) into Eq. (11) and remembering that the numerical Reynolds

number scales as one, it yields:

$$n_{P,\infty} = \rho_\infty c_\infty^2 \tag{16}$$

Eq. (16) tells us that in the asymptotic limit, the normalization parameter n_P scales as $\rho_\infty c_\infty^2$ which leaves us with two options: either $n_P = \rho c^2$ or $n_P = P$. The choice was made to use $n_P = \rho c^2$ in the asymptotic limit (it was found to behave well as shown in Section 5) which ,we believe, is more representative of the flow type. This definition is only valid in the asymptotic limit and the purpose of this paper is to define a viscosity coefficient μ that is valid for a wide range of Mach numbers. Thus, it is proposed to define the high-order viscosity coefficient μ_e as follows:

$$\mu_e = h^2 \frac{\max(\tilde{D}_e, J)}{(1 - f(M))\rho c^2 + f(M)\rho||\vec{u}||^2} \tag{17}$$

where $f(M)$ is a function of the local Mach number M with the following properties:

$$\begin{cases} f(M) \to 0 \text{ as } M \to 0 \\ f(M) \to 1 \text{ as } M \geq 1 \end{cases} \tag{18}$$

The choice of the function $f(M)$ is not fixed and a few examples are available in the literature. (REF) proposed the simple definition $f(M) = \min(M, 1)$ which meets the conditions of Eq. (18). Another definition for $f(M)$ was proposed by (REF):

$$f(M) = \tag{19}$$

All of the numerical results presented in Section 5 were obtained by using $f(M) = \min(M, 1)$ which is simple to implement. A convergence test for a subsonic flow over a 2-D cylinder will show that this definition of $f(M)$ yields the correct behavior in the asymptotic limit. The definition of the high-order viscosity coefficient $\mu_e(\vec{r}, t)$ should behave well for complex flow where a near incompressible regime coexists with a supersonic flow domain since $f(M)$ is function of the local Mach number.

For clarity purpose, the full definition of the viscosity coefficient $\mu(\vec{r}, t)$ is recalled:

$$\begin{cases} \mu(\vec{r}, t) = \max(\mu_{max}(\vec{r}, t), \mu_e(\vec{r}, t)) \\ \text{where } \mu_{max}(\vec{r}, t) = \frac{h}{2}(||\vec{u}|| + c) \\ \text{and } \mu_e(\vec{r}, t) = h^2 \frac{\max(\bar{D}_e, J)}{(1 - f(M))\rho c^2 + f(M)\rho||\vec{u}||^2} \\ \mu(\vec{r}, t) = \kappa(\vec{r}, t) \end{cases} \tag{20}$$

These viscosity coefficients are valid for both the multi-D Euler equations with variable and constant area and are employed with the dissipative terms detailed in Eq. (11). The reader will notice that, through the derivation, none assumption was made on the type of equation of state besides the convexity condition on the entropy function s. The remaining of this paper (Section 5) will focus on demonstrating that the definition of the viscosity coefficient given in Eq. (20) is indeed well-scaled in the asymptotic limit and that shocks are still well resolved.

8

4. Solution Techniques Spatial and Temporal Discretizations

In order to detail the partial and temporal discretization used for this study, the system of equations presented in Section 1 is considered under the following form:

$$\partial_t U + \vec{\nabla} \cdot F(U) = S \tag{21}$$

where U is the vector solution, F is a conservative vector flux and S is a vector source that can contain some relaxation source terms and non-conservative terms.

4.1. Spatial and Temporal Discretizations

The system of equation given in Eq. (21) is discretized using a continuous Galerkin finite element method and high-order temporal integrators provided by the MOOSE framework.

4.1.1. CFEM

In order to apply the continuous finite element method, Eq. (21) is multiplied by a smooth test function ϕ, integrated by part and each integral is split onto each finite element e of the discrete mesh Ω bounded by $\partial\Omega$, to obtain a weak solution:

$$\sum_e \int_e \partial_t U \phi - \sum_e \int_e F(U) \cdot \vec{\nabla}\phi + \int_{\partial\Omega} F(U)\vec{n}\phi - \sum_e \int_e S\phi = 0 \tag{22}$$

The integrals over the elements e are evaluated using quadrature-point rules. The Moose framework provides a wide range of test function and quadrature rules: trapezoidal and Gauss rules among others. Linear Lagrange polynomials will be used as test functions and should ensure second-order convergence for smooth functions. The order of convergence will be demonstrated.

4.1.2. Temporal integrator

The MOOSE framework offers both first- and second-order explicit and implicit temporal integrators. In all of the numerical examples presented in Section 5, the time-dependent term $\int_e \partial_t U \phi$ will be evaluated using the second-order temporal integrator BDF2. By considering three converged solutions, U^{n-1}, U^n and U^{n+1} at three different time t^{n-1}, t^n and t^{n+1}, respectively, it yields:

$$\int_e \partial_t U \phi = \omega_0 U^{n+1} + \omega_1 U^n + \omega_2 U^{n-1} \tag{23}$$

$$\text{with } \omega_0 = , \omega_1 = \text{ and } \omega_2 =$$

9

4.2. Boundary conditions

The boundary conditions will be treated by either using Dirichlet or Neumann conditions. The multi-D Euler equations are wave-dominated systems that require great care when dealing with boundary conditions. It is often recommended to use the characteristic equations to compute the correct flux at the boundaries. Our implementation of the boundary conditions will follow the method described in [6] that was developed for Ideal Gas and Stiffened Gas equation of states. For each numerical solution presented in Section 5, the type of boundary conditions used will be specified.

4.3. Solver

A Free-Jacobian-Newton-Krylov (FJNK) method is used to solve for the solution at each time step.

5. Numerical Results

This section aims at validating our approach detailed in Section 3.2 that focused on deriving a viscosity coefficient behaving well in the asymptotic limit. It is proposed to run both 1- and 2-D simulations. The 1-D simulations consist of liquid water and steam flowing in a convergent-divergent nozzle. This test is interesting for multiple reasons: a steady-state is reached, it can be performed for liquid and gas phases and an analytical solution of the steady-state solution is available. Numerical results for the challenging Leblanc shock tube are also shown (REF). Subsonic flows of a gas over a 2-D cylinder and a hump are simulated and results are shown for various far-field Mach numbers. Numerical results of a supersonic flow in a compression corner are provided to illustrate the capabilities of the new definition in the supersonic case. Convergence studies are performed when an analytical solution is available. For each simulation, informations relative to the boundary conditions and the equation of state will be provided. All of the numerical solution presented in this section are run with the second-order temporal integrator $BDF2$ and linear polynomials test function and integrated with a Gauss second-order quadrature rule.

5.1. Liquid water in a 1-D divergent-convergent nozzle

The liquid water phase is simulated using the Stiffened gas equation of state (REF). The following parameters are used:
The simulation consists of a 1 convergent-divergent nozzle with the following equation, $A(x) = 1 + 0.5\cos(2\pi x/L)$, where $L = 1m$ is the length of the nozzle. At the inlet, a stagnation pressure boundary condition is used: the stagnation pressure and temperature are set to $P_0 = 1MPa$ and $T_0 = 453K$, respectively. At the outlet, only the static pressure is specified, $P_s = 0.5MPa$. Details about the theory related to the inlet and outlet boundary conditions can be found in (REFS). Initially, the temperature is uniform and set equal to the stagnation temperature and the pressure linearly decreases from the stagnation pressure to

309 the static one. Finally, the liquid is assumed at rest. The Stiffened Gas equation
310 of state is used to model liquid water with the parameters provided in Table 1.

Table 1: Stiffened Gas Equation of State parameters for liquid water.

γ	C_v $(J \cdot kg^{-1} \cdot K^{-1})$	P_∞ (Pa)	q $(J \cdot kg^{-1})$
2.35	1816	10^9	-1167.10^3

311   Plots of the pressure, velocity and density are given at steady-state and
312 during the transient. The viscosity coefficients are also plotted but only at
313 steady-state. Since a steady-state analytical solution is available to us (REF),
314 a convergence study is performed in order to demonstrate the accuracy of the
315 entropy viscosity method. For the liquid phase, the solution corresponds to a
316 low-Mach regime case: the flow is isentropic and the final solution does not
317 display any shock or discontinuity. This is a good test to assess the behavior of
318 the new definition of the viscosity coefficient proposed in Eq. (20).
319 Plots of the velocity, pressure, density and viscosity coefficients at steady-state
320 are given in Fig. 1a, Fig. 1b, Fig. 1c and Fig. 1d, respectively. The exact solution
321 is also plotted for comparison. The mesh used is uniform and has 50 cells. The
322 final solution being smooth, a coarse mesh should be sufficient to capture the
323 main features.

(a) Velocity solution at steady-state.

(b) Density solution at steady-state

(c) Pressure solution at steady-state.

(d) Viscosity coefficients at steady-state.

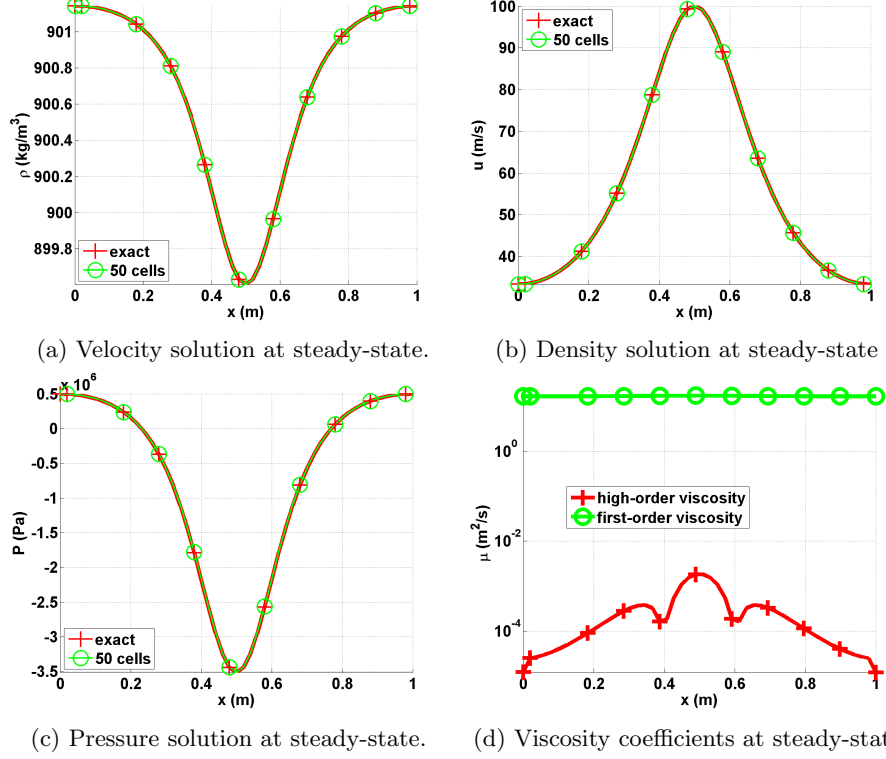Figure 1: Steady-state solution for liquid phase in a 1-D convergent-divergent nozzle with an uniform mesh of 50 cells.

The numerical and exact solutions of the velocity, pressure and density given in Fig. 1 for a fairly coarse mesh (50 cells) perfectly overlap: it is noted the symmetry of the numerical solution with respect to the nozzle throat located in $x = 0.5m$. The second-order viscosity coefficient is very small compare to the first-order one as expected, since the numerical solution is smooth as shown in Fig. 1d. A study convergence was performed using the exact solution as a reference: the L2 norm of the error and the corresponding convergence rates are computed at steady-state on various uniform mesh from 4 to 256 cells. The results for linear polynomials $\mathbb{Q}_1$ is reported in Table 2.

12

Table 2: L2 norm of the error for the liquid phase in a 1-D convergent-divergent nozzle at steady-state.

cells	density	rate	pressure	rate	velocity	rate
4	$3.106397\ 10^{-1}$	—	$5.254445\ 10^{5}$	—	3.288543	—
8	$7.491623\ 10^{-2}$	2.07	$1.636966\ 10^{5}$	1.60	1.823880	0.90
16	$2.079858\ 10^{-2}$	1.80	$4.627338\ 10^{4}$	1.75	$4.990605\ 10^{-1}$	1.83
32	$5.329627\ 10^{-3}$	1.90	$1.180287\ 10^{4}$	1.92	$1.261018\ 10^{-1}$	1.93
64	$1.341583\ 10^{-3}$	1.94	$2.967104\ 10^{3}$	1.98	$3.160914\ 10^{-2}$	1.99
128	$3.359766\ 10^{-4}$	1.99	$7.428087\ 10^{2}$	1.99	$7.907499\ 10^{-3}$	1.99
256	$8.403859\ 10^{-5}$	1.99	$1.857861\ 10^{2}$	1.99	$1.977292\ 10^{-3}$	1.99

It is observed that the convergence rate for the L2 norm of the error is 2: the entropy viscosity method conserves the high-order accuracy when the numerical solution is smooth, and the new definition of the entropy viscosity coefficient seems to behave as expected in the low Mach limit.

5.2. Steam in a 1-D divergent-convergent nozzle

The results of this section are obtained using the exact same 1-D geometry, initial condition and boundary conditions as in Section 5.1. The Stiffened gas equation of state is still used but with different parameters that are given in Table 3.

Table 3: Stiffened Gas Equation of State parameters for steam.

γ	$C_v\ (J \cdot kg^{-1} \cdot K^{-1})$	$P_\infty\ (Pa)$	$q\ (J \cdot kg^{-1})$
1.43	1040	0	2030.10^{3}

The pressure difference applied between the inlet and outlet will make the steam accelerates through the nozzle and result in the formation of shock in the divergent part. The behavior is different from what is observed for the liquid water phase in Section 5.1 because of the liquid to gas density ratio that is of 1000. The objective of this section is to show that using the new definition of the viscosity coefficient in Eq. (20), the shock can be correctly resolved and all spurious oscillations removed. The steady-state numerical solution is shown in Fig. 2 and was run with a mesh of 1600 cells.

(a) Velocity solution at steady-state.

(b) Density solution at steady-state

(c) Pressure solution at steady-state.
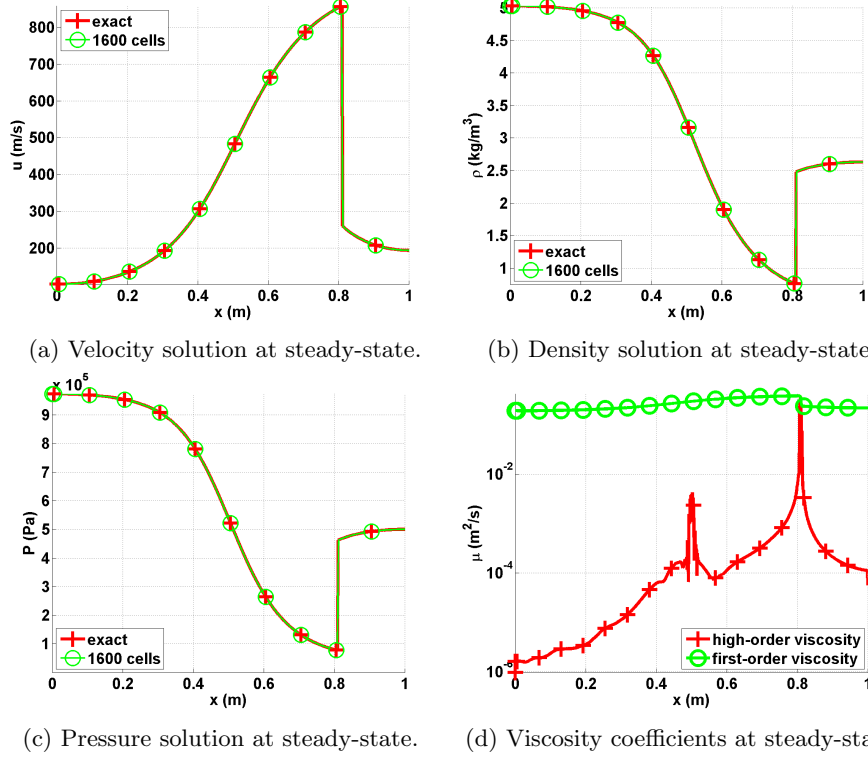
(d) Viscosity coefficients at steady-state.

Figure 2: Steady-state solution for vapor phase in a 1-D convergent-divergent nozzle.

The steady-state solution of the density, velocity and pressure are given in Fig. 2a, Fig. 2b and Fig. 2c. The steady-solution displays a shock around $x = 0.8m$ and match the exact solution. In Fig. 2d, the first- and second-order viscosity coefficients are log plotted at steady-state: the second-order viscosity coefficient is peaked in the shock region around $x - 0.8m$ as expected, and saturate to the first-order viscosity coefficient. The profile also displays another peak at $x = 0.5m$ that corresponds to the position of the sonic point for a 1-D convergent-divergent nozzle: this particular point is known to develop small instabilities that are detected when computing the jumps of the pressure and density gradients. Anywhere else, the second-order viscosity coefficient is small. In order to prove convergence of the numerical solution of the exact solution, a convergence study was performed. Because of the presence of a shock, second-order accuracy cannot be achieved. However, the convergence rate is known and expected to be of 1/2 when computing the L2 norm of the error. Results are provided in ...

14
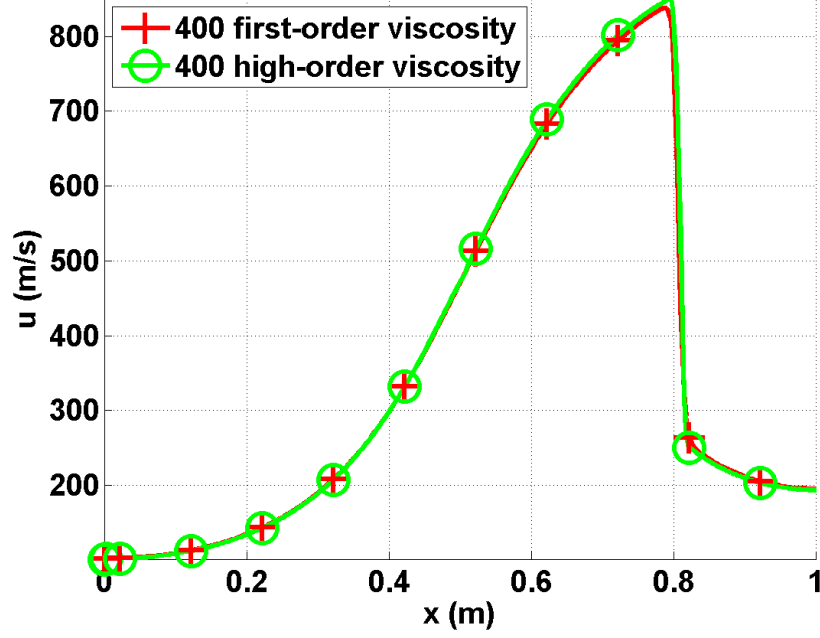
Figure 3: Velocity profile at steady-state with the first- and second-order viscosity for a mesh with 400 cells.

In Fig. 3, the steady-state velocity profile is plotted when using the first- and second-order viscosity coefficients: the main difference between the two numerical solution is in the resolution of the shock around $x = 0.8m$. The first-order viscosity coefficient is by definition more dissipative and will smooth out the solution. In the other hand, the high-order viscosity better resolves the shock and allow high-order accuracy away from the shock region. It is also noted that the numerical solution obtained with the first-order viscosity coefficient is satisfying: this is due to the nature of the solution that contains a standing shock, and thus, will force the shock formation.

Table 4:   L2 norm of the error for the 1-D Leblanc test at $t = 4.s$.

cells	density	rate	pressure	rate	velocity	rate
500	$3.106397\ 10^{-1}$	$-$	$5.254445\ 10^5$	$-$	3.288543	$-$
1000	$7.491623\ 10^{-2}$	0.64781	$1.636966\ 10^5$	0.58793	1.823880	0.89392
2000	$2.079858\ 10^{-2}$	0.70756	$4.627338\ 10^4$	0.53448	$0.53448\ 10^{-1}$	0.77533
3000	$5.329627\ 10^{-3}$	0.64117	$1.180287\ 10^4$	0.58506	$0.58506\ 10^{-1}$	0.72276
4000	$1.341583\ 10^{-3}$	0.58965	$2.967104\ 10^3$	0.56103	$0.56103\ 10^{-2}$	0.60112
5000	$3.359766\ 10^{-4}$	0.54925	$7.428087\ 10^2$	0.55095	$0.55095\ 10^{-3}$	0.55351
6000	$8.403859\ 10^{-5}$	0.31882	$1.857861\ 10^2$	0.44813	$0.44813\ 10^{-3}$	0.15305
7000	$8.403859\ 10^{-5}$	0.51148	$1.857861\ 10^2$	0.52587	$0.52587\ 10^{-3}$	0.50216
8000	$8.403859\ 10^{-5}$	0.50469	$1.857861\ 10^2$	0.52459	$0.52459\ 10^{-3}$	0.50189
9000	$8.403859\ 10^{-5}$	0.51019	$1.857861\ 10^2$	0.51622	$0.51622\ 10^{-3}$	0.52773

(a) Density solution at $t = 4.0s$.

(b) Velocity solution at $t = 4.0s$

(c) Pressure solution at $t = 4.0s$.

(d) Viscosity coefficients at $t = 4.0s$.
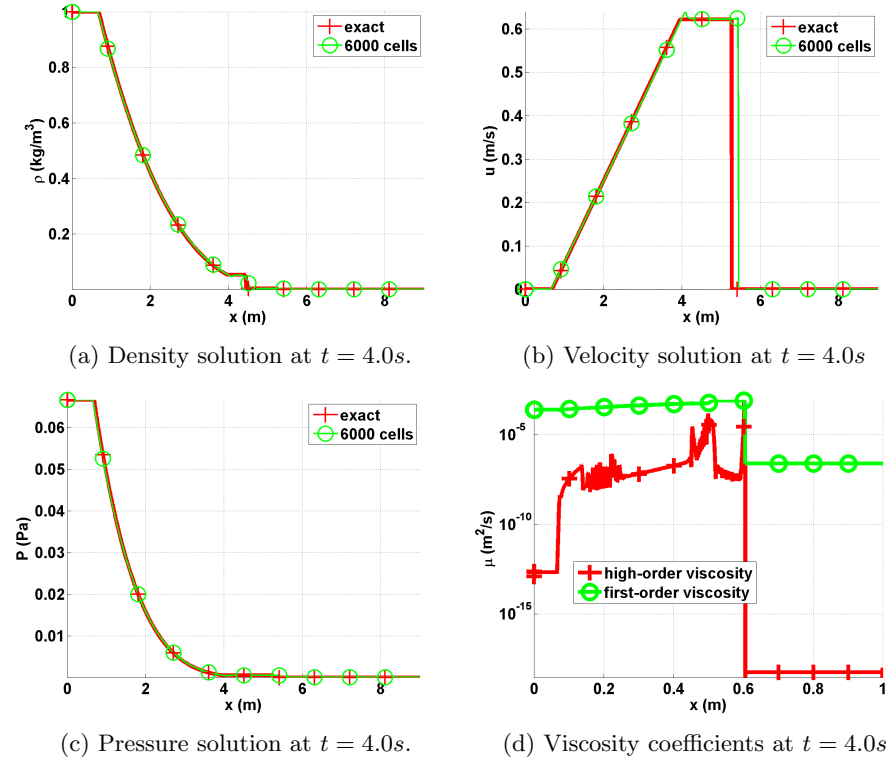
Figure 4: Steady-state solution for vapor phase in a 1-D convergent-divergent nozzle.

(a) Velocity solution at steady-state.

(b) Density solution at steady-state

(c) Presolution at steady-state.
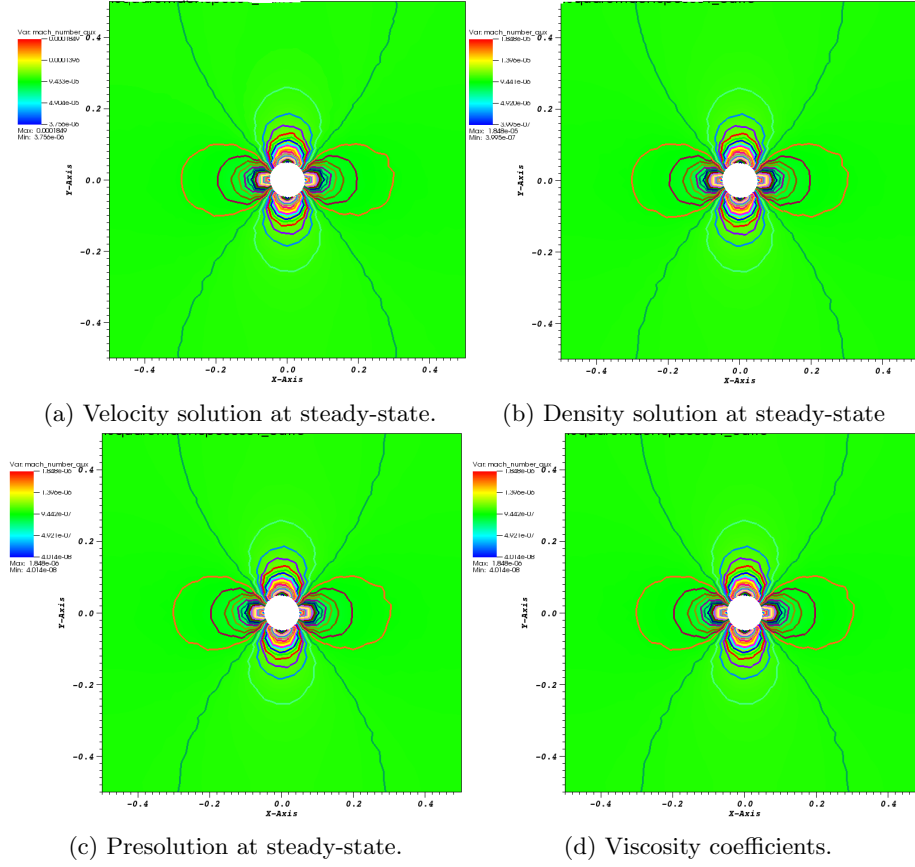
(d) Viscosity coefficients.

Figure 5: Steady-state solution for vapor phase in a 1-D convergent-divergent nozzle.
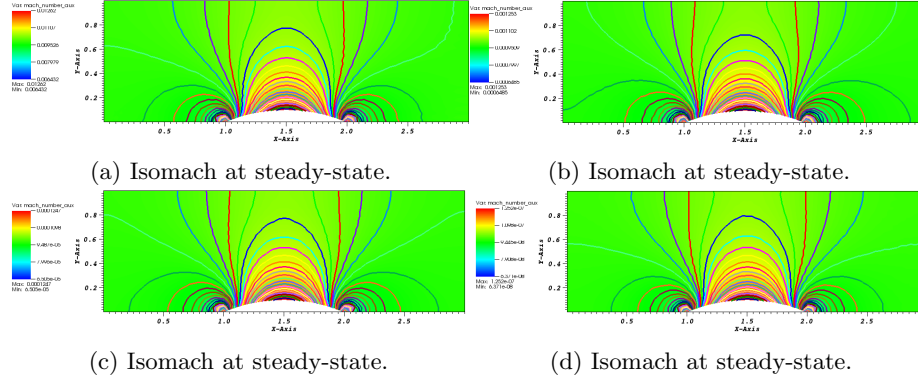
5.5. Subsonic flow over a 2-D hump

(a) Isomach at steady-state.

(b) Isomach at steady-state.

(c) Isomach at steady-state.

(d) Isomach at steady-state.

Figure 6: Steady-state solution for a flow in a 2-D compression corner.

5.6. Supersonic flow in a compression corner

(a) Mach solution at steady-state.

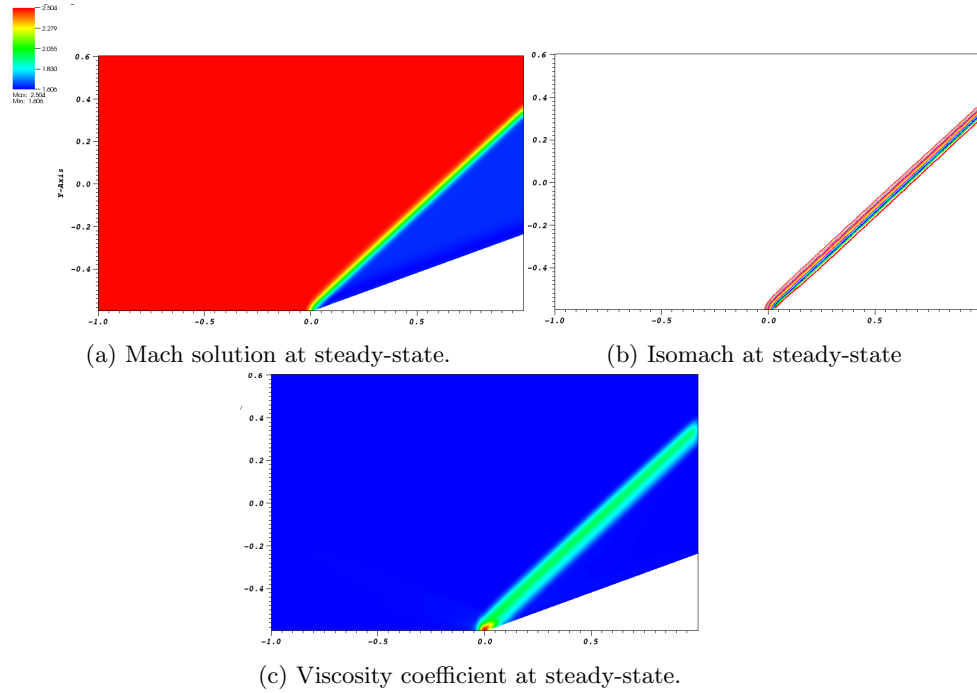(b) Isomach at steady-state

(c) Viscosity coefficient at steady-state.

Figure 7: Steady-state solution for a flow in a 2-D compression corner.

6. Conclusions

Acknowledgments

References

[1] *Implementation of the entropy viscosity method with the discontinuous Galerkin method*, Valentin Zingan, Jean-Luc Guermond, Jim Morel, Bojan Popov, Volume 253, 1 January 2013, Pages 479-490

[2] *Viscous regularization of the Euler equations and entropy principles*, Jean-Luc Guermond and Bojan Popov, under review.

[3] *Entropy viscosity method for nonlinear conservation laws*, Jean-Luc Guermond, R. Pasquetti, B. Popov, J. Comput. Phys., 230 (2011) 4248-4267.

[4] *Entropy Viscosity Method for High-Order Approximations of Conservation Laws*, J-L. Guermond, R. Pasquetti, Lecture Notes in Computational Science and Engineering, Springer, Volume 76, (2011) 411-418.

[5] *Entropy-based nonlinear viscosity for Fourrier approximations of conservation laws*, J.-L. Guermond, R. Pasquetti, C.R. Math. Acad. Sci. Paris 346 (2008) 801806.

[6] *The discrete equation method (DEM) for fully compressible, two-phase flows in ducts of spatially varying cross-section.* R.Berry, R.Saurel, O. LeMetayer, Nuclear Engineering and Design 240 (2010) 3797-3818.

[7] *Riemann Solvers and numerical methods for fluid dynamics.* E.F. Toro, 2nd Edition, Springer.

[8] *On positivity preserving finite volume schemes for Euler equations*, Perthane B. and Shu C-W., Numer. Math., 73(1):119-130, 1996.

20